Optimization of Reflectron for Kinetic and Mechanistic Studies with Multiplexed Multiple Tandem (MSⁿ) Time-of-flight Mass Spectrometry

Yong Jin Bae, So Hee Yoon, Jeong Hee Moon,[†] and Myung Soo Kim[*]

Department of Chemistry, Seoul National University, Seoul 151-742, Korea. [*]E-mail: myungsoo@snu.ac.kr
[†]Medical Proteomics Research Center, KRIBB, Daejeon 305-806, Korea

Photoexcitation of a precursor ion inside a cell floated at high voltage installed in a tandem time-of-flight (TOF) mass spectrometer provides triple tandem mass spectrometric information and allows kinetic and mechanistic studies. In this work, the factors affecting, or downgrading, the performance of the technique were identified. Ion-optical and computational analyses showed that an optimum instrument could be designed by utilizing a reflectron with linear-plus-quadratic potential inside. Theoretical predictions were confirmed by tests with instruments built with different ion-optical layout. With optimized instruments, masses of intermediate ions in the consecutive dissociation of a precursor ion could be determined with the maximum error of ±5 Da. We also observed excellent agreement in dynamical parameters (critical energy and entropy) for the dissociation of a model peptide ion determined by instruments with different ion-optical layout operated under optimum conditions. This suggests that these parameters can be determined reliably by the kinetic method developed previously when properly designed and operated tandem TOF instruments are used.

Key Words: Tandem TOF, MSⁿ, LPQ reflectron, Peptide photodissociation, Dissociation kinetics and dynamics

Introduction

In time-of-flight (TOF) mass spectrometry for ions generated by matrix-assisted laser desorption/ionization (MALDI),[1-4] it is usual to utilize both delayed extraction and reflectron to achieve good time resolution for ions formed in the ion source ('prompt ions'). Specifically, prompt ions are time-focused at the object position of the reflectron – the first time-focusing position – by delayed extraction and refocused by the reflectron at its image position (the second time-focusing position, detector position). Reflectrons with linear potential inside are most popular, which will be called L-reflectron. $d_1 + d_2 = 4\ell$ is the well-known time-focusing condition for L-reflectron.[5] Here d_1 is the distance between the object point and the reflectron entrance, d_2 is that between the reflectron exit and the image point, and ℓ is the penetration depth of an ion in the reflectron. A reflectron with quadratic potential inside, to be called Q-reflectron ('parabolic reflectron', ref. 6), can also be used for high resolution TOF. A salient feature of Q-reflectron is that the flight time of an ion inside the reflectron is unaffected by its kinetic energy. Hence, an ion beam time-focused at the reflectron entrance is refocused at the exit, resulting in the time-focusing condition $d_1 = 0$ and $d_2 = 0$.

Reflectron is also utilized as the second analyzer in TOF-based tandem mass spectrometry.[7-9] When L-reflectron is tuned for a prompt ion, the time-focusing condition is not met for its dissociation products formed in field-free regions outside the source. Product ion time resolution can be improved either by stepping the reflectron voltage or by using a voltage lift cell.[10,11] In contrast, good time resolution for product ions can be achieved with Q-reflectron without instrumental modification.

Recently, we built ultraviolet photodissociation (UV-PD) tandem TOF mass spectrometers to study the dissociation char-

acteristics of peptide ions upon electronic excitation.[12,13] We decided not to use L-reflectron because of the difficulty mentioned above. We also thought that Q-reflectron would be inadequate because the ideal position for PD laser irradiation is close to the detector position. Instead, we used a reflectron with both linear and quadratic potential components, which we called linear-plus-quadratic (LPQ) reflectron. Since we did not have any knowledge on the order of magnitude of the lifetimes of photo-excited peptide ions, we designed instruments with sufficiently long d_1 by using a reflectron with a rather small Q component.[12,13] With this reflectron, unit mass resolution was achieved for product ions formed by post-source decay (PSD)[14] and PD. Also, monoisotopomeric selection of a precursor ion could be done by synchronizing PD laser pulse with ion pulse.

In a subsequent work,[15] we installed a voltage-floatable cell and irradiated a precursor ion (m_1^+) beam with PD laser inside the cell. Our aim was to separate the same product ions (m_2^+) formed inside (in-cell components, I) and outside (post-cell components, P) the cell and hence to obtain kinetic information. In actual voltage-on spectra, however, each m_2^+ peak was observed to split into more than two components, viz. additional components appeared between I and P. They were due to consecutive reactions, $m_1^+ \rightarrow m_i^+ \rightarrow m_2^+$, their first steps occurring inside the cell and the second steps outside, and were called consecutive components (C). A set of all the intermediate ions (m_i^+) involved in the formation of each m_2^+ is basically triple tandem mass spectrometric information. Since reaction intermediate monitoring[16] could be done simultaneously for all m_2^+, the technique was called 'multiplexed PD-MS³.[17]

Our method for kinetic analysis[18] utilizes YPSD (sum of product ion intensities normalized to that of the precursor ion) in PSD and the ratio CPD ≡ Σ[P]/(Σ[I] + Σ[C]) (Σ represents summation over product ions) in PD-MS³. Absence of mass discri-

mination – the same transmission for all ions – is one of the re-quirements for a successful kinetic study. Another requirement is low background noise level because $\Sigma[P]$ or $\Sigma[I] + \Sigma[C]$ can become very small depending on the magnitude of the dissociation rate constant. Even though the mass calibration for m_i^+ of each C component is a requirement for mechanistic studies, this was virtually impossible with the above LPQ instrument.[15]

Time separation of I, C, and P components in PD-MS[3] occurs during their flight in the field-free regions and inside the reflectron. Since the time separation inside L-reflectron more or less counterbalances that in the field-free regions, it is inadequate as an analyzer for MS[3]. Time separation in Q instruments will be larger and also easier to calculate than in L and LPQ instruments because such a counterbalancing is absent. This was confirmed with a Q instrument[17] built as an effort to improve the performance of PD-MS[3] for kinetic and mechanistic studies. Mass accuracy of ± 4 Da was achieved for intermediate ions with this instrument, making it useful for mechanistic study. Using the Q-instrument, we also wanted to perform kinetic studies for peptide ion dissociation and hence to cross-check the dynamical information (critical energy (E_0) and entropy ($\Delta S^{\ddagger}$)) obtained by the LPQ instrument.[18] However, the Q instrument was found to be less than ideal for kinetic study due to the presence of higher background noise level than in the LPQ instrument and the difficulty to eliminate mass discrimination.

In this work, we found through ion-optical analysis that the spatial distribution of ions falling on the detector was responsible for the problems observed with the Q instrument and that the problems became manageable when the L component was added, viz. by using an LPQ reflectron. We also found that the main problem of the previous LPQ instrument[15]–difficulty to mass-calibrate m_i^+–could be remedied simply by increasing its Q component. Based on the findings, a new LPQ instrument (instrument 2) was built and the old one (instrument 1) was improved. Construction of another LPQ instrument (instrument 2) was intentional. That is, we wanted to test the reliability of the dynamical information obtained with the original LPQ instrument by cross-checking with the results from the new instrument with different ion-optical layout. Results are reported in this paper.

Experimental

Layout of instrument 1 after modification is essentially the same as reported previously[15] except that L-to-Q ratio has been changed. Overall layout of instrument 2 is similar even though its details are somewhat different from instrument 1. A schematic drawing of the instruments is shown in Figure 1.

Each instrument consists of a MALDI source with delayed extraction, a deflection system, an ion gate, a voltage-floatable PD cell, an LPQ-reflectron, and a detector. A deflector is installed in front of the reflectron to guide ion beams to the detector. 1.0 cm diameter aperture in the deflector is larger than the aperture (0.5 cm diameter) in the PD cell such that all the ions passing the cell can enter the reflectron. Even though the detector has an effective diameter of 40 mm (Burle, Lancaster, PA), an aperture at the reflectron exit restricts its effective area. The PD cell assembly consists of four apertures with grid E1-E4, with E1 and
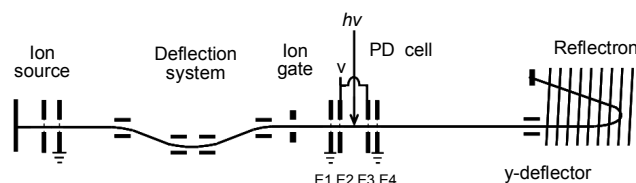

Figure 1. A schematic drawing of the LPQ instruments.

E4 grounded and E2 and E3 floated at the same high voltage. E1-E2, E2-E3, and E3-E4 distances are 4, 11, and 4 mm, respectively. PD laser passes between E2 and E3 and crosses a precursor ion beam perpendicularly.

A nitrogen laser (MNL205-C, Lasertechnik Berlin, Germany) is used for MALDI. The ion gate is turned on to record PSD and PD spectra. In PD experiment, 193 nm pulse of an excimer laser (PSX-100, MPB Communication Inc., Montreal, Quebec) or 266 nm pulse of a Nd:YAG laser (Surelite II-10, Continuum, Santa Clara, CA) is synchronized with the lowest mass isotopomer pulse of a precursor ion beam. The laser-off spectrum is subtracted from the laser-on spectrum to get the PD spectrum.

Samples. The peptides used in this work, YPFVEPI and Y_6, the matrices, 2,5-dihydroxybenzoic acid (DHB) and α-cyano-4-hydroxycinnamic acid (CHCA), and other chemicals were purchased from Sigma (St. Louis, MO). The method to prepare MALDI samples was the same as described previously.[18]

Ion-optical Analysis

General. In a previous section, mass discrimination, background noise level, intermediate ion mass calibration, and separation of I, P, and C components were mentioned as the criteria for successful kinetic and mechanistic studies with PD-MS[n]. Let us take the ion beam direction in the field-free region in front of the reflectron as the x-axis (see Figure 2). y-axis will be defined as the direction of deflection by the deflector installed in front of the reflectron. It is evident that the third and fourth criteria are related to the ion motion along the x-axis. The first two criteria are related to the y motion, as will be explained below.

We mentioned in the preceding section that the entrance aperture of the reflectron is sufficiently large such that all the ions, both the precursor and product ions, that pass the PD cell do enter the reflectron. Even in such a case, mass discrimination can still occur if the spatial spread of ions falling on the detector is wider than its effective y-length, i.e. it is a y problem. Let us now consider the second criterion, viz. background noise. Chemical (particle) noise is the main contributor to the background noise level in our spectra because most of the electrical noises are eliminated in signal handling.[13] We will assume that most of the chemical noises are either negligible (such as cosmic ray) or can be eliminated (such as those due to particles generated by surface collision of ions and neutrals) by minor instrumental adjustments. This leaves product ions spontaneously formed inside the reflectron as the main source of the background noise. Let us define D_y as the displacement of an ion along the y direction during its motion inside the reflectron. It can be shown by SIMION[19] calculations that a product ion formed inside the re-
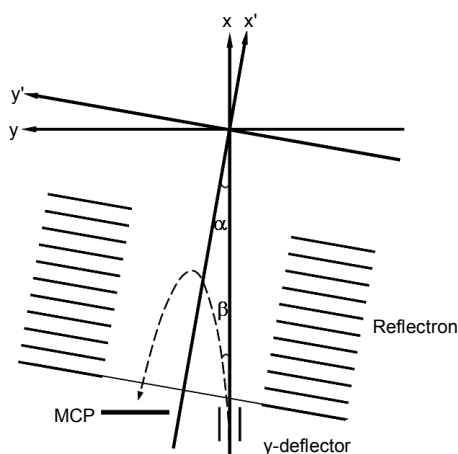
Figure 2. Coordinate convention. The direction of ion beam before it enters the reflectron is the x-axis. The y-axis, perpendicular to x, lies on the plane of deflection. A deflector in front of the reflectron deflects ion beam by an angle β. The central axis of the reflectron is the x'-axis, which is tilted from x by an angle α. The y'-axis is perpendicular to x'.

flectron comes out with smaller D_y than m_1^+. Then, if all the product ions (m_2^+) formed before m_1^+ enters the reflectron have larger D_y than m_1^+, background chemical noise can be somewhat reduced by adjusting y-deflector potential. Otherwise, efforts to reduce the background chemical noise would induce mass discrimination. The above argument shows that the second criterion also concerns the y motion of ions. For a definite understanding of the problems concerning mass discrimination and background noise in Q- and LPQ-reflectrons, D_y inside ideal reflectrons under the MS^2 condition (zero potential on the cell) will be derived in this section. D_y under the MS^3 condition is more complicated and hence will not be derived here. We will just mention our finding from SIMION calculations that the above problems disappear in MS^3 when the same problems in MS^2 are adequately handled.

Let us suppose that a precursor ion (m_1^+ with m/z m_1) with kinetic energy K_0 moving along the x-axis dissociates to m_2^+ and m_3 in the field-free region. Ignoring the kinetic energy release, the kinetic energy of m_2^+ is given as follows.

$$K = (m_2/m_1) K_0 \tag{1}$$

Both m_1^+ and m_2^+ move along the x-axis with the same velocity (v_0).

$$v_0 = (2K_0/m_1)^{1/2} \tag{2}$$

Let us suppose that m_2^+ is deflected by an angle β due to the y-deflector located in front of the reflectron. It is well known that β is inversely proportional to mass.

$$\beta \propto m_2^{-1} \tag{3}$$

Reflectron. Let us consider a cylindrically symmetric reflectron and take its central axis as x'. The axis on the deflection plane perpendicular to x' will be defined as the y'-axis, as shown

in Figure 2. We will generalize the problem by assuming that the x'-axis is tilted from the x-axis by an angle α as shown in the figure. Taking into account the deflection by the y-deflector, the entering ion beam will make an angle $\alpha + \beta$ with respect to the x'-axis. Since the potential inside the reflectron is given as a function of x', viz. V(x'), the force on m_2^+ inside the reflectron acts only along the x' direction, $F(x') = - dV/dx'$. Reflectrons with the following potential inside will be considered.

$$V(x') = c_1 x' + c_2 x'^2 \tag{4}$$

Master equation for D_y. The ion motion inside the reflectron is easier to solve on the x'y'-plane than on the xy-plane because there is no force acting along the y' direction. Velocity components of the entering m_2^+ beam are as follows.

$$v_{0,x'} = (2K_0/m_1)^{1/2} \cos(\alpha + \beta) \tag{5}$$

$$v_{0,y'} = (2K_0/m_1)^{1/2} \sin(\alpha + \beta) \tag{6}$$

The kinetic energy due to the x' motion of the entering m_2^+ beam is as follows.

$$K_{x'}(entrance) = (m_2/m_1) K_0 \cos^2(\alpha + \beta) \tag{7}$$

Let us define t_r as the flight time of m_2^+ inside the reflectron. The expression for t_r can be derived by analyzing the motion along x'. Since m_2^+ moves with a constant velocity along y' ($v_{0,y'}$) inside the reflectron, its displacement along the y'-axis at the reflectron exit becomes $v_{0,y'} \times t_r$. By projecting this to the y-axis, the following master equation for D_y is obtained.

$$D_y = (2K_0/m_1)^{1/2} t_r \sin(\alpha + \beta) \cos\alpha \tag{8}$$

Q-reflectron. Previously,[12] we presented the expression for t_r of an ion with mass m that enters an LPQ-reflectron perpendicularly ($\alpha = 0$ and $\beta = 0$) with the kinetic energy K. By substituting eqn. (7) into that expression and m_2 into m, t_r^{LPQ} for m_2^+ can be derived as follows.

$$t_r^{LPQ} = (2m_2/ec_2)^{1/2} [\pi/2 - \sin^{-1}\{1 + 4c_2 (m_2/m_1) \\ \times K_0 \cos^2(\alpha + \beta) / ec_1^2\}^{-1/2}] \tag{9}$$

t_r for Q-reflectron can be obtained by inserting $c_1 = 0$ in the above equation.

$$t_r^Q = \pi (m_2/2ec_2)^{1/2} \tag{10}$$

Then, D_y in Q-reflectron, D_y^Q, becomes as follows.

$$D_y^Q = \pi [(K_0/ec_2)(m_2/m_1)]^{1/2} \sin(\alpha + \beta) \cos\alpha \tag{11}$$

When y-deflector is not used ($\beta = 0$), the following expression for D_y^Q is obtained.

$$D_y^Q = (\pi/2) [(K_0/ec_2)(m_2/m_1)]^{1/2} \sin 2\alpha \tag{12}$$

Since $D_y^Q \propto m_2^{1/2}$, m_2^+ falls on the detector closer to the

x-axis than m_1^+. In this case, it will be difficult to sufficiently reduce the background chemical noise without inducing mass discrimination.

Without tilting the reflectron ($\alpha = 0$) and with small β, the following expression is obtained from eqn. (11).

$$D_y^Q = \pi \, [(K_0/ec_2)(m_2/m_1)]^{1/2} \, \beta \qquad (13)$$

Since $\beta \propto m_2^{-1}$ (eqn. (3)), D_y^Q is proportional to $m_2^{-1/2}$. That is, D_y^Q of m_2^+ is larger than that of m_1^+ and increases as m_2 decreases. In this case, it will be possible to reduce the background chemical noise by adjusting y-deflector potential. It will be shown in the next section, however, that mass discrimination in Q-reflectron is difficult to avoid unless an instrument with very large dimension is built.

One can not cancel the above two effects by using a Q-reflectron with $\alpha \neq 0$ and $\beta \neq 0$. Here, the influence of β will be dominant at very low mass while that of α will become important at higher mass. Then, product ions will fall on the detector at both sides of m_1^+.

LPQ-reflectron. By inserting eqn. (9) into eqn. (8), D_y for LPQ-reflectron, D_y^{LPQ}, can be obtained.

$$D_y^{LPQ} = 2[(K_0/ec_2)(m_2/m_1)]^{1/2} \times [\pi/2 - \sin^{-1}\{1 + 4c_2 \, (m_2/m_1)$$
$$K_0 \cos^2(\alpha + \beta) \, / \, ec_1^2\}^{-1/2}] \times \sin(\alpha + \beta) \cos\alpha \qquad (14)$$

Without the y-deflector ($\beta = 0$), D_y^{LPQ} becomes as follows.

$$D_y^{LPQ} = [(K_0/ec_2)(m_2/m_1)]^{1/2} \times [\pi/2 - \sin^{-1}\{1 + 4c_2 \, (m_2/m_1)$$
$$K_0 \cos^2\alpha \, / \, ec_1^2\}^{-1/2}] \, \sin2\alpha \qquad (15)$$

The terms in the first and second brackets decrease as m_2 decreases. That is, all product ions fall on the detector closer to the x-axis than m_1^+, a bad situation.

D_y^{LPQ} without reflectron tilting ($\alpha = 0$) is as follows.

$$D_y^{LPQ} = 2[(K_0/ec_2)(m_2/m_1)]^{1/2} \times [\pi/2 - \sin^{-1}\{1 + 4c_2 \, (m_2/m_1)$$
$$K_0 \cos^2\beta \, / \, ec_1^2\}^{-1/2}] \times \sin\beta \cong 2[(K_0/ec_2)(m_2/m_1)]^{1/2}$$
$$[\pi/2 - \sin^{-1}\{1 + 4c_2 \, (m_2/m_1) \times K_0 \cos^2\beta \, / \, ec_1^2\}^{-1/2}] \, \beta$$
$$(16)$$

The term in the first bracket and β result in the mass dependence of $m_2^{-1/2}$. That is, D_y^{LPQ} increases as m_2 decreases, viz. product ions fall on the detector farther from the x-axis than m_1^+, just as for Q-reflectron. On the other hand, the term in the second bracket decreases as m_2 decreases, resulting in smaller D_y^{LPQ}.

Now, let us compare the general expression ($\alpha \neq 0$ and $\beta \neq 0$) for D_y^{LPQ} (eqn. (14)) with that for D_y^Q (eqn. (11)). The only difference between the two is the presence of the term in the second bracket of eqn. (14), as found for the untilted reflectron. Narrower spread of product ion signals due to this term in LPQ-reflectron means that a detector with smaller y length can be used.

With a proper design, it may also be possible to keep D_y^{LPQ} for product ions equal to or larger than that for m_1^+, and hence to reduce the chemical noise.

SIMION Calculations

The ion-optical analysis presented in the preceding section is very useful for understanding the reasons for the enhanced chemical noise level and for the difficulty to eliminate mass discrimination in the Q instrument constructed previously.[17] The result also suggests that such difficulties will become less serious for properly designed LPQ instruments. However, the master equation (eqn. (14)) derived for LPQ-reflectron looks too complicated, and will become even more complicated for MS[3], to use for instrument design. The equation has been derived under the assumption that the electrostatic force acts only along the x' direction. In actual reflectron, force also acts along the y' and z' directions due to field penetration. Another factor that has not been taken into account is the ion spread along the y-axis arising from kinetic energy release. To take all these factors into account, we utilized SIMION calculations in actual instrument design.

Distances between the ion source and the end of the deflection system, between this end and the center of the PD cell, between this center and the reflectron entrance, and between the reflectron exit and the detector were fixed. They were 912, 89, 249, and 20 mm, respectively, for instrument 2 (corresponding values for instrument 1 were 607, 105, 281, and 20 mm, respectively). The length of the reflectron in instrument 2 was the same as in instrument 1, i.e. 527 mm. The reflectron consisted of 31 circular apertures (electrodes) with the external diameter of 130 mm. The internal diameters of the first, second, and third apertures were 80, 80, and 70 mm, respectively, while those for the remainder were 60 mm. 25.0 kV was applied to the last electrode of the reflectron and a voltage divider circuit distributes the potential to other electrodes. 20.0 kV DC and 1.5 kV AC were applied to the sample plate in the MALDI source. m/z 1000 was taken for the prompt ion, which was assumed to be generated with the initial velocity in the range 500 - 1000 m sec^{-1} and within $\pm60^{\circ}$ with respect to the x-axis. In PD, 3 kV was taken as the cell potential. Finally, the kinetic energy release of 0.1 eV was assumed in the formation of product ions.[20]

In actual calculations, we first chose a position somewhere near the PD cell as the first time-focusing point and hence specified d_1. With d_1 and d_2 specified, LPQ potential, viz. c_1 and c_2, was calculated using an equation reported previously.[12] The potential at each electrode in the reflectron was adjusted iteratively to obtain the above LPQ potential. The instrument was tuned such that prompt ions were time-focused at the chosen first time-focusing position. It was confirmed that time-focusing was also achieved at the second time-focusing position (detector position). Then, SIMION calculations were performed to determine time separation of I, C, and P components in MS[3] and D_y. α, β, and d_1 are the parameters that can be varied for optimization. In the actual instrument, β can be easily varied by changing y-deflector potential. In contrast, mechanical and electrical changes are needed to vary α and d_1, respectively. In a previous PD-MS[3] work,[15] it was shown that the P component of any m_2^+

96   *Bull. Korean Chem. Soc.* **2010**, Vol. 31, No. 1

Yong Jin Bae et al.

Table 1. Flight time separation (in nsec) between P and C components ($\Delta t_{PC} = t_P - t_C$) in the LPQ instrument with $d_1 = 130$ mm and $\alpha = 0.3^{\circ}$ calculated with various combinations of m_2 and m_i at 3 kV cell voltage.[a]

m_i	m_2							
	100	200	300	400	500	600	700	800
900	15.6	14.4	13.9	13.7	13.6	13.5	13.4	13.3
800	35.4	32.2	31.1	30.5	30.2	30.0	29.8	
700	60.0	54.4	52.5	51.4	50.9	50.5		
600	91.4	82.7	79.7	78.2	77.2			
500	132.9	120.1	115.7	113.6				
400	189.8	171.8	165.8					
300	273.3	248.2						
200	408.9							

[a]m/z of m_1 is 1000.

could be readily identified *via* simple spectral shift. Here we will report the flight times of I (t_I) and C (t_C) components as their differences from that of P component (t_P), viz. as $\Delta t_{PI} = t_P - t_I$ and $\Delta t_{PC} = t_P - t_C$, respectively.

The first thing found by SIMION calculations was that Δt_{PI} changed from negative to positive as the product ion mass increased when the center of the PD cell was located after the first time-focusing position. This was probably responsible for the difficulty in intermediate ion mass calibration experienced with the previous LPQ instrument.[15] Δt_{PI} was positive regardless of product ion mass when the PD cell center was located in front of the first time-focusing position, i.e., when d_1 was shorter than the distance (249 mm) between the cell center and the reflectron entrance. Also, Δt_{PI} increased as d_1 got shorter, i.e., as the contribution of the quadratic component increased. For example, Δt_{PI} for m_2^+ with m/z 300 was 434.1 and 239.8 nsec when d_1 was 30 and 130 mm, respectively.

Δt_{PC} was calculated for the LPQ instrument with $d_1 = 130$ mm with various combinations of m_2 and m_i. The results are listed in Table 1. It is to be noted that Δt_{PC} changes rather systematically with changes in m_2 and m_i, suggesting a possibility to mass-assign m_i^+. Δt_{PC} for a given neutral loss ($m_i - m_2$) decreases rapidly as m_2 increases. Poor time separation at large m_2 is not fatal because the resolution of an LPQ instrument improves and the number of consecutive channels decreases as m_2 increases. Even though Δt_{PI} and Δt_{PC} are the largest with Q-reflectron ($d_1 = 0$), we do not favor this reflectron based on our previous experience and our mathematical findings in the preceding section. Also, as the distance between the PD cell and the first time-focusing position gets longer, the time spread of m_1^+ pulse at the PD cell gets broader, a potential problem in monoisotopomeric selection of m_1^+. In addition, our experience with the previous Q instrument was that its resolution in MS^n was not as good as that of LPQ probably because the time spread of an entering product ion beam caused by kinetic energy release could not be counterbalanced by Q-reflectron. We calculated Δt_{PI}, Δt_{PC}, and the temporal width of the precursor ion at the PD cell center using various d_1 values, took into account the time resolution measured with our previous LPQ instrument, and decided to adopt $d_1 = 130$ mm as a compromise.
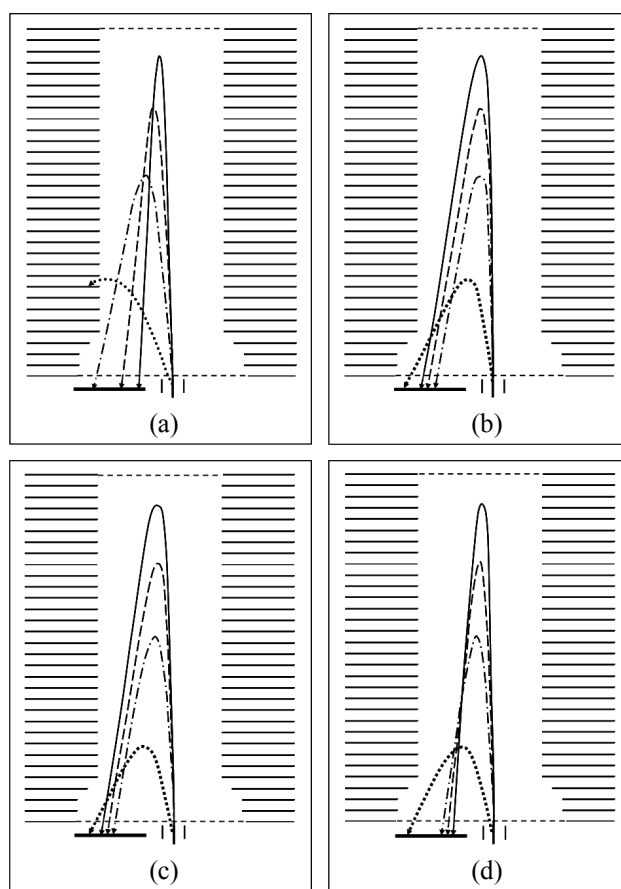
Figure 3. y-distributions of m_1^+ (m/z 1000, ——) and m_2^+ with m/z 100 (⋯⋯), 400 (—·—·), and 700 (– – –) falling on the detector calculated for Q- and LPQ-reflectrons with various combinations of d_1 and α. (a) $d_1 = 0$ (Q) and $\alpha = 0$, (b) $d_1 = 0$ (Q) and $\alpha = 0.7^{\circ}$, (c) $d_1 = 130$ mm (LPQ) and $\alpha = 0.6^{\circ}$, and (d) $d_1 = 130$ mm (LPQ) and $\alpha = 0.3^{\circ}$.

y-Distributions of m_1^+ and some m_2^+ falling on the detector were calculated for LPQ-reflectrons with various combinations of d_1 and α. In such calculations, β was adjusted to guide ion beams to the detector as well as possible. Some of the typical results are shown in Figure 3. y-distributions of I components calculated with 3 kV on the cell were similar and will not be shown. Figure 3(a) shows y-distributions calculated with an untilted Q-reflectron ($d_1 = 0$ and $\alpha = 0$). Severe y-deflection at small m_2 makes it difficult to avoid mass discrimination. Mass discrimination can be avoided by tilting the Q-reflectron as shown in Figure 3(b). Then, product ions fall on both sides of m_1^+, making it difficult to reduce background chemical noise. The same occurred for the LPQ-reflectron with $d_1 = 130$ mm when the tilting angle as large as 0.6° was used (Figure 3(c)). Finally, displacements for all m_2^+ could be made larger than that of m_1^+ by using smaller tilting angles, as demonstrated with $\alpha = 0.3^{\circ}$ in Figure 3(d). In this case, y-distribution of m_2^+ is narrower than in Figure 3(a), suggesting that mass discrimination can be avoided. The results from SIMION calculations are in good qualitative agreement with those predicted by simple ion-optical analysis presented in the preceding section. It is to be mentioned that our goal of reducing background chemical noise and eliminating mass discrimination could be achieved with various com-

binations of d_1 and α, even though we decided to use LPQ-reflectron with $d_1 = 130$ mm and $\alpha = 0.3°$ in this work.

Performance of the LPQ Instrument

Mass discrimination. We built and tested the performance of LPQ-reflectrons with several different combinations of d_1 and α including our choice ($d_1 = 130$ mm and $\alpha = 0.3°$). PSD spectra for the peptide ion $[YPFVEPI + H]^+$ recorded with a range of y-deflector potential (V_y) in the LPQ instrument with $d_1 = 130$ mm and $\alpha = 0.3°$ are shown in Figure 4. Product ion peak heights in each spectrum were normalized to that of m_1^+. It is to be noted that the relative intensities of product ions are essentially the same over the V_y range of 50 - 60 V. In contrast, intensities of low mass product ions look stronger at lower V_y (e.g. $V_y = 30$ V), while weaker at higher V_y (e.g. $V_y = 80$ V). The results can be explained based on our finding in the preceding section that D_y for m_2^+ is larger than that of m_1^+ in this reflectron and increases as m_2 decreases. At $V_y = 30$ V, some of m_1^+ fails to arrive at the detector such that low mass product ions look stronger after normalization. At $V_y = 30$ V, we also observed that very high mass product ions became weaker after normalization. This occurred because D_y for high mass product ions became smaller than that of m_1^+ at this V_y, as confirmed through SIMION calculations. At $V_y = 80$ V, D_y values for low mass product ions become large such that some of them fail to arrive at the detector, resulting in weaker intensities after normalization than at $V_y = 50 - 60$ V. It is to be emphasized that V_y-dependence of the spectral pattern in Figure 4 is consistent with our theoretical and computational findings and that mass discrimination in this instrument can be eliminated by adjusting V_y.

Background chemical noise. To see the influence of the deflector potential on background chemical noise in these spectra, two spectra, those recorded with V_y of 60 V and 80 V, are reproduced in Figure 5(a) and 5(b), respectively, after 30-fold magnification. It is to be noted that the background noise level in high product ion mass range increases as V_y increases. We have mentioned that m_2^+ formed from m_1^+ inside the reflectron has smaller D_y than m_1^+. D_y of such ions will also increase as V_y increases. Then, more of such ions, especially those with large m/z, will fall on the detector, resulting in higher background chemical noise level as observed in Figure 5(b). We also recorded PSD spectra of $[YPFVEPI + H]^+$ using reflectrons with different combinations of d_1 and α. A spectrum (normalized and magnified by 30) recorded with a reflectron with $d_1 = 30$ mm and $\alpha = 1.5°$ is shown in Figure 5(c). According to SIMION calculations, product ions fall on the detector at both sides of m_1^+ with this reflectron. Since V_y was adjusted to eliminate mass discrimination for product ions with smaller D_y than m_1^+, product ions formed inside the reflectron would be detected more efficiently. That is, higher background level in Figure 5(c) than in 5(a) is consistent with the results from the ion-optical analysis and SIMION calculation in the preceding sections. Finally, it is to be mentioned that the background chemical noise level in PD was similar to that in PSD unless excessively intense laser was used for PD.

Component separation in MS³. Normalized 193 nm PD spectrum of $[YPFVEPI + H]^+$ is shown in Figure 6(a). Splitting patterns of some product ion peaks with 3 kV on the PD cell are
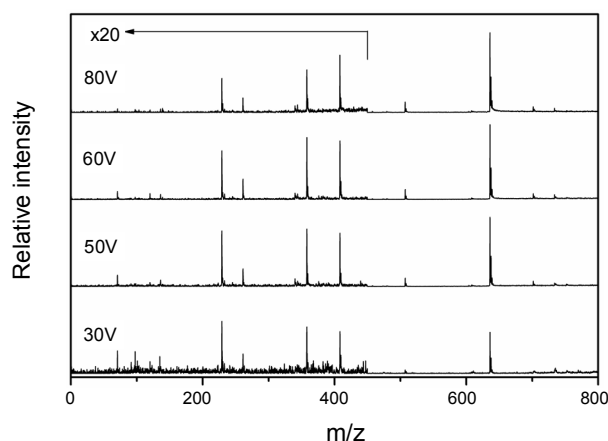

Figure 4. PSD spectra for $[YPFVEPI + H]^+$ recorded with the y-deflector potential (V_y) of 30, 50, 60, and 80 V in the LPQ instrument with $d_1 = 130$ mm and $\alpha = 0.3°$.
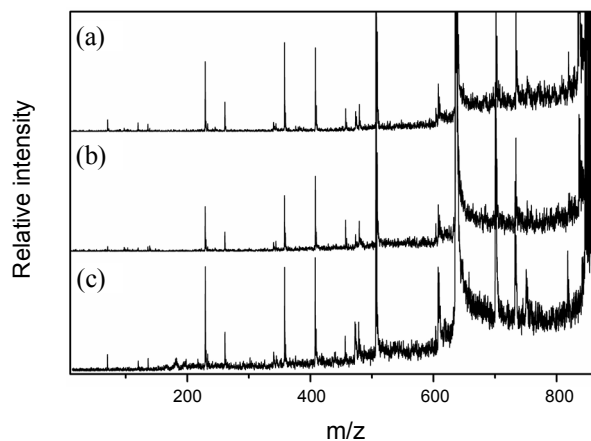

Figure 5. PSD spectra for $[YPFVEPI + H]^+$ recorded with the y-deflector potential (V_y) of 60 and 80 V in Figure 4 are shown in (a) and (b), respectively, after 30-fold magnification. A spectrum (normalized and magnified by 30) recorded with a reflectron with $d_1 = 30$ mm and $\alpha = 1.5°$ is shown in (c) after 30-fold magnification.

shown as insets. In Table 2, Δt_{PI} values for various product ions measured from the 3 kV-on PD spectrum are compared with the corresponding values obtained by SIMION calculations. Experimental and computed Δt_{PI} values are a little different, even though general trends are similar, suggesting that the potential inside the reflectron is a little different from the original intention. Mechanical and electrical imprecision in the homebuilt instrument is probably responsible for the difference.

Intermediate ion mass calibration. We attempted to mass-calibrate intermediate ions for C components of each m_2^+ by comparing experimental and calculated Δt_{PC} values. The theoretical expression for Δt_{PC} in Q instrument had been reported previously.[17] Δt_{PC} in LPQ instrument will be different from this due to the flight time difference inside the reflectron, which can be calculated by eqn. (9). We adjusted c_1 of the reflectron potential such that the experimental and calculated Δt_{PI} values became the same and used this c_1 to calculate Δt_{PC} as a function of m_i.

Table 2. Experimental and calculated flight time separation (in nsec) between P and I components ($\Delta t_{PI} = t_P - t_I$) in 193 nm PD spectrum of [YPFVEPI + H]$^+$ obtained at 3 kV cell voltage using the LPQ instrument with d_1 = 130 mm and $\alpha = 0.3^\circ$.

| $m_2{}^+$	Experiment	Calculation
P	683.5	716.0
F	449.5	468.7
Y	405.0	419.6
PF-CO	258.2	262.1
y_2	243.9	246.5
b_2	211.1	210.7
y_3	129.1	135.8
b_3	104.4	109.4
a_4	87.4	80.3
b_4	77.0	70.8

Table 3. Masses (in Da) of intermediate ions ($m_i{}^+$)^{a,b} involved in the consecutive formation of various $m_2{}^+$ from [YPFVEPI + H]$^+$.

$m_2{}^+$	$m_i{}^+$	correct mass	Ref. 17 experimental mass	Ref. 17 mass error	This work experimental mass	This work mass error
P	EP	227.1	224.6	−2.5	224.2	−2.9
F	FV-CO	219.1	221.3	2.2	217.0	−2.1
Y	b_2	261.1	262.7	1.6	261.7	0.6
PF-CO	PF	245.1	245.8	0.7	243.9	−1.2
y_2	y_3	358.2	361.2	3.0	357.1	−1.1
	y_4	457.3	460.0	2.7	457.0	−0.3
PF	PFV	344.2	348.0	3.8	339.7	−4.5
b_2	b_3	408.2	410.5	2.3	404.2	−4.0
	b_5	636.3	638.4	2.1	632.2	−4.1
PFV	PFVE	473.2	477.1	3.9	470.0	−3.3
	y_6	701.4	698.7	−2.7	701.3	−0.1
y_3	y_6	701.4	700.5	−0.9	699.2	−2.2
b_3	a_4	479.3	477.6	−1.7	482.1	2.8
	b_4	507.3	506.9	−0.4	510.8	3.6
	b_5	636.3	632.0	−4.3	641.2	4.9
PFVE	b_5	636.3	633.8	−2.5	638.0	1.7
	y_6	701.4	699.2	−2.2	705.8	4.4
a_4	a_5+1	609.3	612.1	2.8	609.3	0.0
	b_5	636.3	635.6	−0.7	635.5	−0.8
b_4	b_5	636.3	633.5	−2.8	631.6	−4.7

^{a}From 193 nm PD spectrum recorded with 5 kV cell voltage. ^{b}Non-overlapping peaks were chosen.

Then, m_i for each C component observed in the experiment was estimated by comparing its Δt_{PC} with the calculated result. Intermediate ions in consecutive formation of various $m_2{}^+$ from [YPFVEPI + H]$^+$ were identified in our previous study[17] with a Q-instrument at 5 kV cell voltage. The same experiment was done in this work using the LPQ instrument (instrument 2). The results for non-overlapping peaks are compared with those from the previous assignments in Table 3. It is to be noted that the
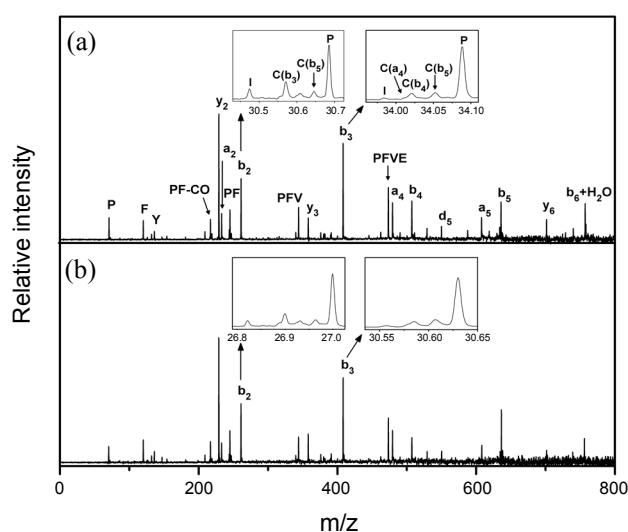
Figure 6. Normalized 193 nm PD spectrum of [YPFVEPI + H]$^+$ recorded with (a) instrument 2 and (b) modified instrument 1. Splitting patterns of some product ion peaks with 3 kV on the PD cell are shown as insets (x-axis of the insets is time-of-flight, in μsec).

intermediate ion mass can be determined with the maximum error of ±5 Da with the present LPQ instrument.

Modification of instrument 1. The previous LPQ instrument (instrument 1)[15] was modified to improve its capability to mass-calibrate intermediate ions in MS^3. We simply increased the quadratic component in the reflectron potential such that d_1 became 220 mm. Since d_1 in instrument 1 was longer than in instrument 2, Δt_{PI} was a little shorter and the maximum mass error for $m_i{}^+$ was a little larger (±5.3 Da). Normalized 193 nm PD spectrum of [YPFVEPI + H]$^+$ recorded with 3 kV cell voltage in the modified instrument 1 is shown in Figure 6(b). It is to be noted that PD spectra recorded with the two instruments are quite similar. More importantly, 3 kV-on splitting patterns for some product ion peaks shown in insets are also quite similar.

Kinetic data. Details of the method for kinetic analysis for peptide ions were reported previously.[18,21] Briefly, the internal energy distribution ($P_0(E)$) for a peptide ion formed by MALDI was calculated by assuming thermal equilibrium at a temperature T.[4] For a peptide ion without arginine, cleavage of each amide bond forms b- and y-type ions. Hence, many b/y channels compete in the dissociation of a peptide ion. The total dissociation rate constant, $k_{tot}(E)$, was calculated by assuming similar dynamical characteristics for the competing b/y channels. That is, $k_{tot}(E)$ was estimated by multiplying the rate constant for an average channel, $k(E)$, by the number of the amide bond. $k(E)$ was calculated by Rice-Ramsperger-Kassel-Marcus (RRKM) theory[22,23] at specified critical energy (E_0) and entropy ($\Delta S^{\ddagger}$). Using $k(E)$ and $P_0(E)$, theoretical YPSD and CPD were calculated. Calculations were done for nearly one hundred million sets of ($T, E_0, \Delta S^{\ddagger}$). The sets in agreement with the experimental results within error limits were chosen. E_0 and $\Delta S^{\ddagger}$ values were determined by averaging over these sets. In this work, [Y$_6$ + H]$^+$ was chosen as the peptide ion because its dissociation kinetics had been studied previously.[18] CPD data obtained by photodissociation at 193 and 266 nm were used. To narrow down the ran-

Table 4. The critical energy (E_0, in eV) and entropy ($\Delta S^{\ddagger}$, in eu[a]) for the dissociation of $[Y_6 + H]^+$ determined by the modified instrument 1, instrument 2, and the original instrument 1.

	E_0	$\Delta S^{\ddagger}$
Modified instrument 1	0.64 ± 0.10	-25.9 ± 5.8
Instrument 2	0.68 ± 0.09	-24.2 ± 4.6
Original instrument 1[b]	0.63 ± 0.07	-26.3 ± 4.3

[a]1 eu = 4.184 J K^{-1}mol^{-1} [b]Retreatment (see text) of data in ref. 21.

ges of E_0 and $\Delta S^{\ddagger}$, YPSD and CPD measured for $[Y_6 + H]^+$ formed by CHCA- and DHB-MALDI were used. E_0 and $\Delta S^{\ddagger}$ values determined with the modified instrument 1 and instrument 2 are listed in Table 4. Previously,[21] we reported E_0 and $\Delta S^{\ddagger}$ values obtained by the original instrument 1 using CHCA, DHB, and sinapinic acid as matrices. To compare with the present results, kinetic analysis was done using CHCA- and DHB-MALDI data only. The results are also listed in Table 4. Considering that the ion-optical layouts for the three instruments are different and that the instruments were operated and calibrated independently, the agreement among the E_0 and $\Delta S^{\ddagger}$ values determined by these instruments is remarkable. We take the results as partial evidence that our kinetic method is reliable to determine E_0 and $\Delta S^{\ddagger}$ for peptide ion dissociation.

Conclusion

Capability to separate and identify various peaks appearing in voltage-on PD spectra is an important requirement for the kinetic and mechanistic studies with TOF-based PD-MS^n. Absence of mass discrimination and low background noise level are also required for reliable and efficient utilization of the technique. Through theoretical and computational analyses of ion trajectories, we found in this work that these requirements could be met by using a properly designed LPQ reflectron with a deflector in front of it. Performance of the new LPQ instrument built and the old instrument modified following the theoretical guideline was rather satisfactory. As an ultimate test, dynamical parameters for the dissociation of a model peptide ion were determined. Even though the three LPQ instruments used in the kinetic study had somewhat different ion-optical layout and were operated and calibrated independently, the final results were quite similar. We take this as an evidence that most of the experimental factors affecting the reliability of the dynamical parameters determined by our kinetic method have been taken good care of.

References

1. Hillenkamp, F.; Karas, M. *In MALDI MS. A Practical Guide to Instrumentation, Methods and Applications*; Hillenkamp, F., Peter-Katalinić, J., Eds.; Wiley-VCH Verlag GmbH & Co. KGaA: Weinheim, 2007; pp 1-28.
2. Knochenmuss, R.; Zenobi, R. *Chem. Rev.* **2003**, *103*, 441.
3. Dreisewerd, K. *Chem. Rev.* **2003**, *103*, 395.
4. Knochenmuss, R. *Analyst* **2006**, *131*, 966.
5. Cotter, R. J. *Time-of-Flight Mass Spectrometry*; American Chemical Society: Washington, 1997; pp 48-53.
6. Rockwood, A. L. *Proceedings of the 34th Annual Conference on Mass Spectrometry and Allied Topics*; Cincinnati, June 8-13, 1986.
7. Hettick, J. M.; McCurdy, D. L.; Barbacci, D. C.; Russell, D. H. *Anal. Chem.* **2001**, *73*, 5378.
8. Cotter, R. J.; Gardner, B. D.; Iltchenko, S.; English, R. D. *Anal. Chem.* **2004**, *76*, 1976.
9. Vestal, M.; Juhasz, P. *J. Am. Soc. Mass Spectrom.* **1998**, *9*, 892.
10. Spengler, B. *J. Mass Spectrom.* **1997**, *32*, 1019.
11. Suckau, D.; Resemann, A.; Schuerenberg, M.; Hufnagel, P.; Franzen, J.; Holle, A. *Anal. Bioanal. Chem.* **2003**, *376*, 952.
12. Oh, J. Y.; Moon, J. H.; Kim, M. S. *J. Am. Soc. Mass Spectrom.* **2004**, *15*, 1248.
13. Moon, J. H.; Yoon, S. H.; Kim, M. S. *Bull. Korean Chem. Soc.* **2005**, *26*, 763.
14. Kaufmann, R.; Chaurand, P.; Kirsch, D.; Spengler, B. *Rapid Commun. Mass Spectrom.* **1996**, *10*, 1199.
15. Yoon, S. H.; Kim, M. S. *J. Am. Soc. Mass Spectrom.* **2007**, *18*, 1729.
16. Ballard, K. D.; Gaskell, S. J. *Int. J. Mass Spectrom. Ion Processes* **1991**, *111*, 173.
17. Shin, Y. S.; Moon, J. H.; Kim, M. S. *Anal. Chem.* **2008**, *80*, 9700.
18. Moon, J. H.; Yoon, S. H.; Kim, M. S. *J. Phys. Chem. B* **2009**, *113*, 2071.
19. Dahl, D. A. SIMION 3D, version 7.0, Idaho National Labs, Idaho Falls, ID, 2000.
20. Ambihapathy, K.; Yalcin, T.; Leung, H.; Harrison, A. G. *J. Mass Spectrom.* **1997**, *32*, 209.
21. Yoon, S. H.; Moon, J. H.; Kim, M. S. *J. Am. Soc. Mass Spectrom.* **2009**, *20*, 1522.
22. Holbrook, K. A.; Pilling, M. J.; Robinson, S. H. *Unimolecular Reaction*; Wiley: Chichester, U. K., 1996; pp 39-78.
23. Baer, T.; Mayer, P. M. *J. Am. Soc. Mass Spectrom.* **1997**, *8*, 103.